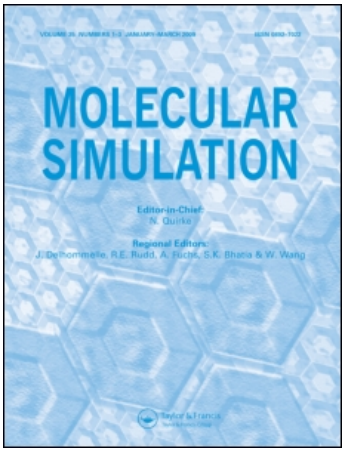

Molecular Simulation
Publication details, including instructions for authors and subscription information:
http://www.informaworld.com/smpp/title~content=t713644482

On the properties of aqueous amide solutions through classical molecular dynamics simulations

S. Aparicio-Martínez[a]; P. B. Balbuena[a]
[a] Artie McFerrin Department of Chemical Engineering, Texas A&M University, College Station, TX, USA

Online publication date: 27 July 2010

To cite this Article Aparicio-Martínez, S. and Balbuena, P. B.(2007) 'On the properties of aqueous amide solutions through classical molecular dynamics simulations', Molecular Simulation, 33: 11, 925 — 938
To link to this Article: DOI: 10.1080/08927020701474422
URL: http://dx.doi.org/10.1080/08927020701474422

Molecular Simulation, Vol. 33, No. 11, September 2007, 925–938

Taylor & Francis
Taylor & Francis Group

On the properties of aqueous amide solutions through classical molecular dynamics simulations

S. APARICIO-MARTÍNEZ† and P. B. BALBUENA*

Artie McFerrin Department of Chemical Engineering, Texas A&M University, College Station, TX 77843, USA

(Received December 2006; in final form May 2007)

The structure and dynamics of infinitely diluted aqueous amide solutions is studied for 13 compounds in the NVT ensemble using classical molecular dynamics simulations. The aim of this work is to provide valuable insights into the effect of amides on liquid water properties in order to understand the amides role in the kinetic inhibition of clathrate hydrate formation in natural gas mixtures. The OPLS-AA forcefield is used to describe the amides, with parameters obtained through fitting of computed B3LYP/6-311 + +g** data when not available in the literature, and the SPC-E model is applied for water molecules. Structural properties of the solutions are analyzed via calculated radial distribution functions and dynamic properties are studied with the computed mean square displacements and velocity autocorrelation functions. Most of the studied compounds show a remarkable structuring effect on the surrounding water with strong interactions resulting from hydrogen bonding between solute and solvent molecules. Hydrophobic and hydrophilic synergistic effects influence the amide–water interaction and the properties of the water solvation shells around amides.

Keywords: Amide; Water; Molecular dynamics; Hydrate inhibitors

1. Introduction

The clathrates of water, so-called hydrates, are inclusion compounds in which a small non-polar guest molecule is enclosed into the interstices of a water lattice [1]. The voids in clathrate cages are larger than in ice phases with each cavity able to accommodate only one guest molecule. These small guest molecules stabilize the hydrogen bonded network through nonbonding repulsive interactions. Two main types of crystalline structures of clathrates are well known: type I (cubic) and type II (face centered cubic), the formation of each type depending upon the size of the guest molecules. It is well known that many of the natural gas constituents may form stable hydrates under the conditions in which the gas is commonly transported through pipelines [2,3]. This constitutes a major problem for the gas industry with considerable economical and safety concerns and thus methods to avoid or delay the hydrate formation are commonly applied in the gas industry [3]. The inhibition of hydrate formation can be done through thermodynamic or kinetic methods. The thermodynamic methods are based in the shifting of the boundaries of phase diagrams and thus reducing the temperature or increasing the pressure at which the hydrate would form [4]. Instead, the kinetic inhibitors interfere with the growth of the crystal structure, slowing the crystallization process [5]. In the natural gas industry, alcohols, mainly methanol and glycols, are commonly used as thermodynamic hydrate inhibitors. Although this kind of thermodynamic inhibitors could prevent the formation of hydrates for indefinite time, they have some serious drawbacks because in order to be effective they have to be used at very high concentrations, as high as 40% for methanol. This is economically very costly [6], environmentally unfriendly and may create additional potential hazards and logistic problems [7]. A promising alternative has been developed in the last years with the discovery of the so-called low dosage inhibitors (LDI) that work according to a kinetic mechanism and are needed in very low concentrations. LDI decrease substantially the inhibition costs and eliminate the aforementioned drawbacks of the thermodynamics inhibitors [8]. Although the mechanism of kinetic inhibition is still not fully understood, it is believed

*Corresponding author. Email: sapar@ubu.es
†Department of Chemistry, University of Burgos, 09001 Burgos, Spain. Email: balbuena@tamu.edu.

Molecular Simulation
ISSN 0892-7022 print/ISSN 1029-0435 online © 2007 Taylor & Francis
http://www.tandf.co.uk/journals
DOI: 10.1080/08927020701474422

that the inhibitors are selectively adsorbed onto active sites in the crystals, thus preventing additional growing [1,9,10]. Hence, LDI generally include organic molecules with sizes and shapes close to the dimensions of the crystal active sites in which they are adsorbed.

The successful LDI inhibition abilities at ppm level concentrations have given rise to a wide academic and industrial interest for the development and screening of new and more efficient compounds. Many of the molecules that have been tested successfully pertain to the amide family such as poly-vinyl-2-pyrrolidinone, one of the first kinetic inhibitors commercially available [11–13].

Considering that the LDI inhibition mechanism is still under discussion and because of the inherent difficulties associated with a systematic experimental screening of wide collections of molecules, theoretical simulations constitute a very valuable tool for these purposes [14]. Thus, molecular simulations can serve on one side to study the mechanism of inhibition at a molecular level, and on the other side, for testing families of potential inhibitors before doing expensive and time-consuming laboratory or field tests.

The understanding of the kinetic inhibition mechanism requires a proper knowledge of the behavior of the inhibitors in water solution, of the intermolecular inhibitor–water interactions, and of the effect of the inhibitors on the complex liquid water hydrogen-bonding network. This goal may be achieved through the use of molecular modeling from which molecular level information may be inferred.

Thus, considering the well known importance of amides as possible candidates for kinetic inhibitors, in this work we study the structure of infinitely dilute amide–water solutions according to classical molecular dynamics (MD) simulations. A group of 10 amides pertaining to different families were selected according to their potential in the LDI field; most of them are monomers of different polymeric LDIs which have shown experimentally high performance as inhibitors and even some of them are commercially available and have been tested in field applications. The information obtained will serve to understand the molecular origin of the factors that control the amide–water interaction, and by extension the LDI mechanism using simple molecules as models instead of the more complex polymeric LDIs.

The studied compounds belong to the families of formamides (formamide, FOR, *N*-methylformamide, NMF and *N*,*N*-dimethylformamide, DMF), acetamides (acetamide, ACE, *N*-methylacetamide, NMA and *N*,*N*-dimethylacetamide), linear amides with vinyl group (acrylamide, ACA), and cyclic amides (2-pyrrolidinone, PYR, 2-piperidinone, PIP, *N*-methyl-2-pyrrolidinone, NMP). We report structural and dynamic data on the properties of water around the amide solute molecules. The very different structures of the amides in this study provide information about the factors that control the solute–solvent interactions and the solution molecular level structure, such as the presence of *N*-substituents of various classes, hence enabling the evaluation of elements that may enhance the performance of kinetic inhibitors.

2. Methods

In the present study, MD simulations in the NVT ensemble were carried out using the DL_POLY package [15]. All the simulations were performed at 298.15 K with the temperature controlled via the Nosé–Hoover thermostat [16]. The equations of motion were solved using the Verlet Leapfrog integration algorithm [17]. Water geometry and amides covalent bonds length were constrained according to the Shake algorithm [18]. Long range electrostatic interactions are treated with the smooth particle mesh Ewald method [19]. The simulated systems consist of cubic boxes of 19 Å side length, in which one amide and 223 water molecules are placed, subjected to periodic boundary conditions in the three spatial directions (density $\sim 0.99\,\mathrm{g\,cm^{-3}}$). All the simulations were done using a cutoff radius of 9.5 Å for the non-bonded interactions. The simulation length was 700 ps, with a time step of 1 fs. The first 100 ps were used for equilibration, which was determined by the absence of systematic drifts in the variation of the potential energy as a function of time. The remaining 600 ps were used for production purposes.

The potential used to mimic water was the extended simple point charge model, SPC/E [20], in which the molecule is assumed to be rigid and three point charges are included. This model performs reasonably well in reproducing the structural and thermodynamic properties and the dynamics of water [21,22].

The description of amides was done according to the so-called Optimized Potential for Liquid Simulations in its *all atom* version, OPLS-AA [23]. This model has been applied successfully in computing liquid state properties of very different types of systems [24–26], including amides [23,27,28]. Most of the amide OPLS-AA parameters required for the computations are available in the literature [23], but for the ACA molecule some parameters are missing. Thus, quantum computations were done using the Gaussian 98 package [29] with density functional theory (DFT) employing the Becke gradient corrected exchange functional [30] in conjunction with the Lee-Yang-Parr correlation functional [31] with three parameters (B3LYP) [32], and the 6-311 + + g** basis set. The optimized structures and atomic charges calculated at B3LYP/6-311 + + g** level for the studied amides are reported in figure 1. These atomic charges were calculated to fit the electrostatic potential according to the Merz–Singh–Kollman [33] method and were used in the MD simulations. For vinyl amides, potential energy scans at the same level of theory were done to determine the forcefield parameters not available in the literature. Lennard–Jones and remaining

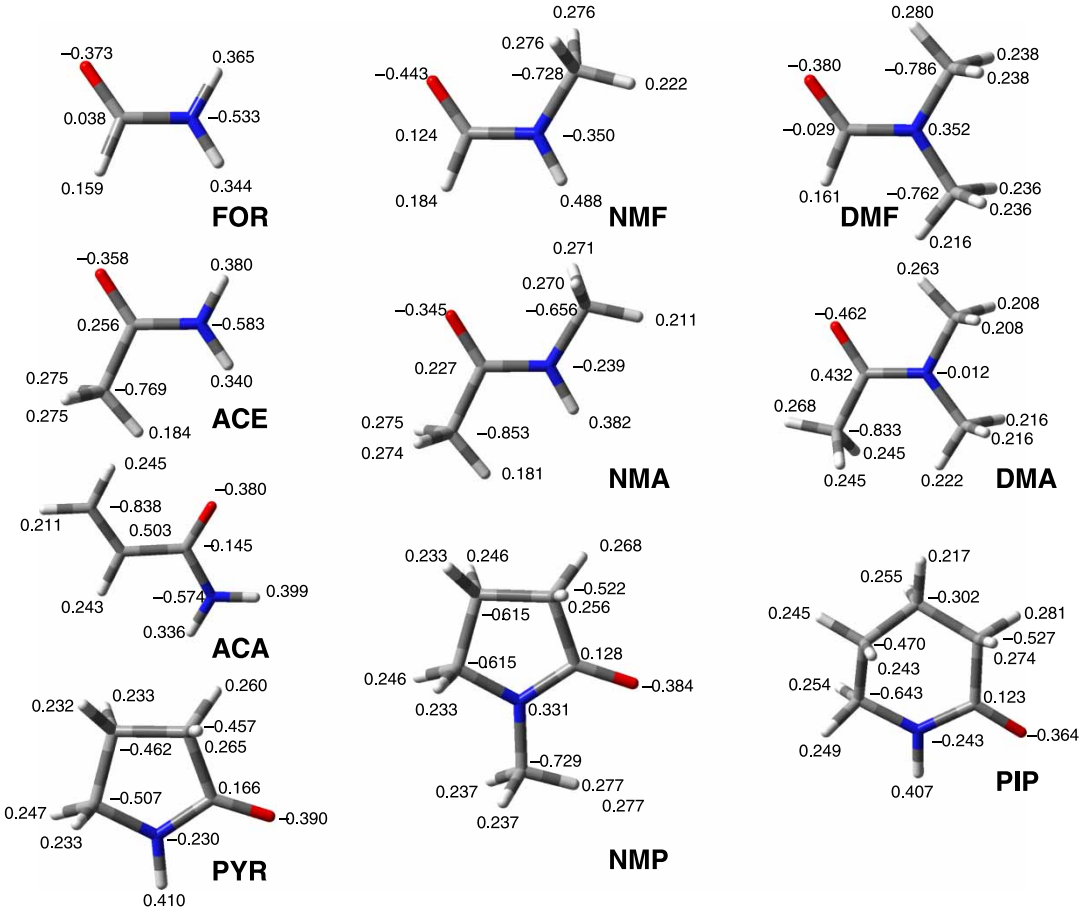

Figure 1. Optimized structures and charges in gas phase calculated with the B3LYP/6-311 + + g** method. Results for NMF, NMA and ACA previously reported in Ref. [34]. Color code: N atoms, blue; O atoms, red; C atoms, dark grey; H atoms, light grey (Colour in online version).

parameters were obtained from the OPLS-AA original work [23]. OPLS-AA does not have a standard way to compute charges (frequently they are fitted to reproduce liquid properties and thus they are basically empirical) [23]. Other forcefields, such as AMBER, use HF instead of DFT for charges calculations, because it is claimed that DFT charges are usually overestimated. In this work we use DFT charges because of the higher quality of B3LYP calculations compared with HF ones. We note that HF calculations on amides such as PYR [35] show charges only slightly lower than those obtained in this work through DFT, showing the reliability of the chosen physical model. Furthermore, the use of OPLS-AA model for solutes together with water SPC/E model instead of other water approaches has proved to be a reliable method to study solvation phenomena in water for a variety of molecules including amides [27,28,36,37].

3. Results and discussion

The amides in this work are classified into families of compounds, and the MD results analyzed separately for these groups of molecules.

3.1 Formamides

The first group (figure 1) corresponds to FOR, NMF and DMF aqueous solutions. These molecules have two main moieties in their structure: the hydrophilic amide group and the hydrophobic methyl group attached to the amide nitrogen (in NMF and DMF). The interaction of these two sites with water determines the effect of the amide on the water–hydrogen bonded network. For NMF, the *trans* isomer, in which the methyl substituent is on the same side of the molecule as the carbonyl oxygen, is predominant both in gas phase and in water solution [34,38,39]. Therefore, we shall limit the study to the *trans* form only. Different conformers may arise from the methyl group rotation; although the staggered conformer reported in figure 1 is the most stable one [40,41], rotational barriers around this methyl group are very small [40,42].

Figure 2 shows the computed radial distribution functions, RDF, for some selected important pairs in these mixtures. The distribution of water around the amide oxygen, figure 2(a), shows a sharp peak in the RDF at very short distances (table 1) pointing to strong hydrogen bonding. The position of the peak is almost unaffected by the type of amide (table 1), only the intensity of the peak

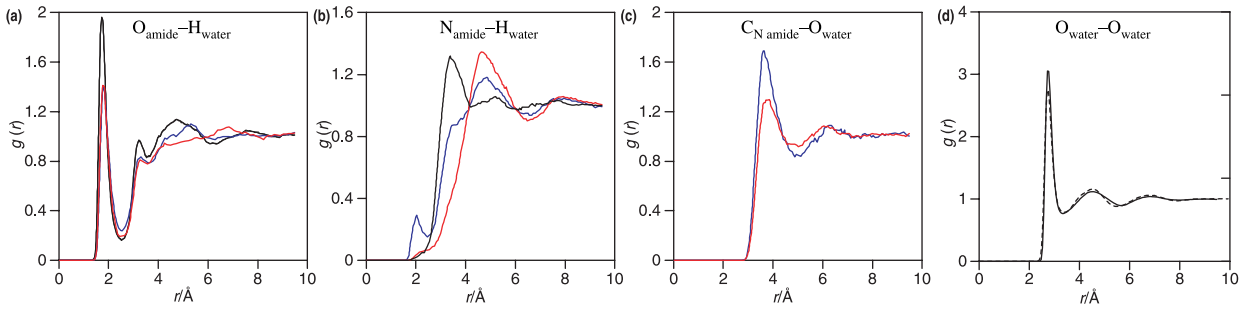

Figure 2. Calculated radial distribution functions, $g(r)$ for amide (formamide family)—water solutions. (—) FOR, (—) NMF, (—) DMF. r = interatomic distance. In (d) and (h): (—) calculated SPC/E and (- - -) experimental neutron diffraction data [47].

changes. The solvation numbers, $n(R)$, are defined as the number of water molecules (i), within a sphere of radius R centered in the j moiety and may be calculated according to equation (1):

$$n(R) = n_{ij}(R) = \rho_{\text{bulk}} \int_0^R g_{ij}(r) 4\pi r^2 \mathrm{d}r \qquad (1)$$

where g_{ij} is the corresponding RDF and ρ_{bulk} the number density of bulk water molecules. The radius R of the first solvation shell is estimated from the position of the first minimum in the corresponding RDF. Solvation numbers are reported in table 1 and decrease slightly going from FOR to DMF, but it can be concluded that two hydrogen bonds are established between water and the amide oxygen. The presence of the methyl substituent in the same side of the molecule such as the carbonyl oxygen for the prevailing *trans* NMF causes certain steric hindrance in the 1 amide: 2 water complexes decreasing the peak height of the O_{amide}—H_{water} radial distribution function (figure 2(a)), and thus the solvation number in the first shell (table 1). To confirm this, the structures and energies of these complexes interacting with water via the carbonyl oxygen were calculated at B3LYP/6-311 + + g** theoretical level and reported in figure 3. The H(water)—O(amide) distances shown in figure 3 for 1 formamide:2 water complexes fall into the hydrogen bonding range, thus confirming the MD results. For FOR, figure 3(a), a simultaneous interaction with the H(nitrogen) is also possible, giving rise to a cyclic structure. This is confirmed by the larger binding energy for FOR/water complexes reported in figure 3 which points to simultaneous double hydrogen bonding of a water molecule with both positions of the amide moiety.

The calculated solvation numbers shown in table 1 for formamides are in agreement with literature quantum and classical simulations [43–45]. OPLS/*united atom* solvation data reported in the literature [46] are different to the OPLS/*all atom* shown in this work which are much closer to the more accurate quantum simulations results. The variation of the solvation number with the size of the shell reported in figure 4(a) indicates that the solvation through the carbonyl oxygen is more effective for FOR than for the *N*-methylsubstituted amides in which the methyl group makes the interaction more difficult.

In figure 2 we also report the RDF for the O_{water}—O_{water} pair for comparative purposes, the calculated functions are

Table 1. Interatomic distances, Å, corresponding to the maximum of the first peak and minimum after the first peak of the radial distribution functions, and solvation numbers, n, defined as the number of water molecules in the first solvation shell, for amide–water solutions (grouped in different families).

	O_{amide}–H_{water}			N_{amide}–H_{water}			$C_{N,amide}$–O_{water}			$C_{N,amide}$–H_{water}		
	Max	*Min*	*n*	*Max*	*Min*	*n*	*Max*	*Min*	*n*	*Max*	*Min*	*n*
FOR	1.73	2.53	2.36	3.38	4.23	16.94						
NMF	1.78	2.53	2.22	4.88	6.58	72.60	3.63	4.88	13.50	3.98	5.18	32.75
DMF	1.78	2.48	1.99	4.68	6.48	68.63	3.83	4.58	9.54	4.33	5.28	32.67
	O_{amide}–H_{water}			N_{amide}–H_{water}			$C_{1,amide}$–O_{water}			$C_{N,amide}$–O_{water}		
	Max	Min	*n*	Max	Min	*n*	Max	Min	*n*	Max	Min	*n*
ACE	1.78	2.63	2.52	3.53	4.43	18.67	3.73	5.63	21.80			
NMA	1.73	2.63	2.38	4.83	6.48	74.90	3.78	5.43	18.54	3.78	5.43	18.70
DMA	1.83	2.63	2.15	5.23	6.68	73.66	3.78	5.38	16.94	3.78	5.33	15.86
	O_{amide}–H_{water}			N_{amide}–H_{water}			$C_{1,amide}$–O_{water}			$H_{N,amide}$–O_{water}		
	Max	Min	*n*	Max	Min	*n*	Max	Min	*n*	Max	Min	*n*
ACA	1.78	2.63	2.60	3.63	4.48	18.84	3.78	5.08	15.41	2.13	2.53	0.70
	O_{amide}–H_{water}			N_{amide}–H_{water}			$H_{N,amide}$–O_{water}			$C_{N,amide}$–O_{water}		
	Max	Min	*n*	Max	Min	*n*	Max	Min	*n*	Max	Min	*n*
PYR	1.78	2.48	2.60	2.18	2.68	1.25	1.63	2.38	1.00			
PIP	1.78	2.63	2.39	2.08	2.58	1.09	1.68	2.38	1.00			
NMP	1.73	2.53	2.22	5.18	7.08	88.84				3.68	5.33	15.97

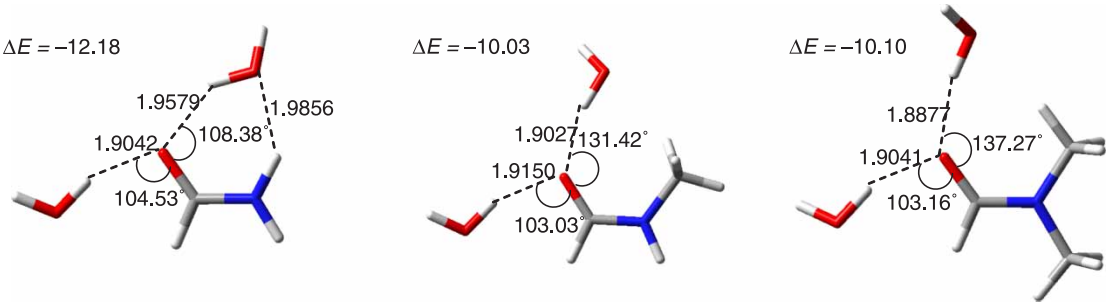

Figure 3. Optimized structures and equilibrium binding energies, ΔE_i, for amide (formamide family) + water complexes calculated at B3LYP/6-311 + + g** level. Interatomic distances in Å, angles in degrees and equilibrium binding energies in kJ mol^{-1}. Color code as in figure 1.

in good agreement with experimental values obtained through neutron diffraction experiments [47], as previous studies have shown [48].

The distribution of water around the amide nitrogen is shown in figure 2(b). The RDF peak shifts to higher interatomic distances (table 1) when the methyl group *N*-substituents are introduced. The positions of the peaks do not suggest the existence of hydrogen bonding with the amide nitrogen; only in formamide solutions hydrogen bonding through the hydrogen attached to the nitrogen may be established (a sharp peak in the RDF($H_{N,amide}$—O_{water}) at 1.83 Å is obtained, not shown). Although the hydrogen bonding through the nitrogen atom is not feasible in DMF and NMF according to the position of the peaks in figure 2(b), a very small feature appears for NMF at around 2.1 Å, in agreement with previous works [43]. Some authors have assigned such feature to weak interactions of the water hydrogen with the nitrogen atom but the RDF indicates that the probability of this kind of interaction is very low. The number of water molecules in the first solvation shell centered in the amide nitrogen increases going from FOR to NMF and DMF (table 1) as a consequence of the increasing solvation shell size because of the *N*-methyl groups. These nitrogen—centered shells are large as it is shown by the *n* values. Figure 2(b) shows that at short distances nitrogen in FOR is better solvated than in the other amides because of the absence of hydrophobic methyl groups present in NMF and DMF.

More detailed information about solvation around the hydrophobic moiety may be obtained through the study of the shells around the *N*-methyl groups in NMF and DMF, figure 2(c). The RDF($C_{N,amide}$—O_{water}) shows peaks at 3.63 Å for NMF and 3.83 Å for DMF, the solvation numbers calculated from the integration of these first peaks (table 1) are lower than the values corresponding to complete clathrate cages (for which the solvation numbers should be 20, 24 or 28) [9]. The values reported in table 1 for the RDF($C_{N,amide}$—H_{water}) are slightly greater than the DFT calculated values for ($C_{N,amide}$—O_{water}), figure 3(c), nevertheless the results point to a distorted hydrogen bonding water network around the hydrophobic amide methyl groups. This hydrophobic interaction is more intense for DMF as it is shown by the lower and less sharp peak in the O_{amide}—H_{water} and $C_{N,amide}$—O_{water} RDFs.

The dynamic properties of these solutions are reported in figure 5. Since the water molecule has the largest part of its mass concentrated in the oxygen atom and the motion of the O and H atoms are strongly correlated in the rigid model, the analysis of water dynamics may be done through the study of the oxygen

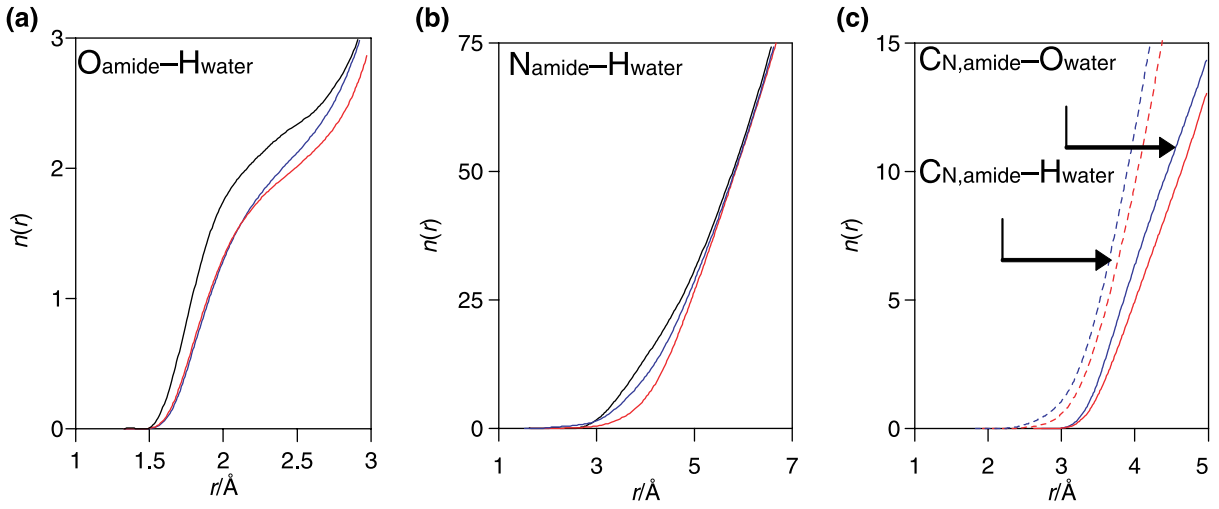

Figure 4. Number of atoms, $n(r)$, within a sphere of radius r for amide (formamides family)—water solutions. The first atom reported in the labels for each plot is the central one. Symbols as in figure 2. r = interatomic distance.

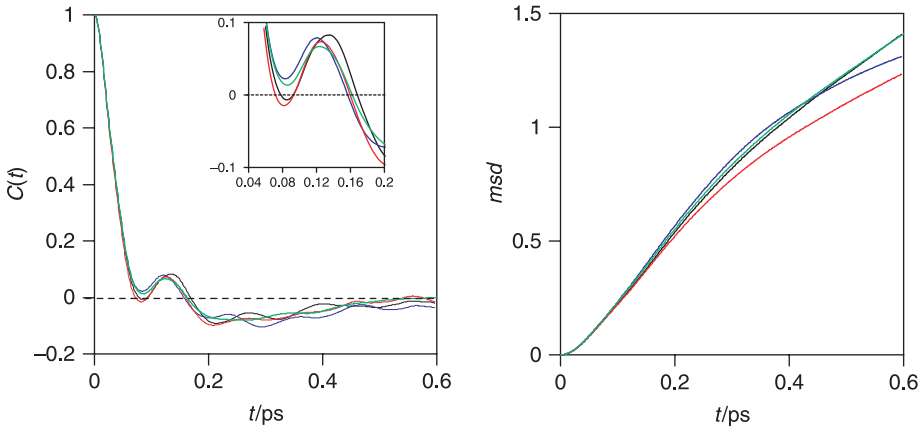

Figure 5. Velocity autocorrelation function, $C(t)$, and mean square displacement, msd/Å[2], of water oxygen atoms for amide (formamide family)—water solutions. t = time. Symbols as in figure 2. Results for pure SPC-E water are also included, (—).

motion only. Water oxygen mean square displacements, msd, are calculated according to equation 2 over the entire number of water molecules and trajectories, for pure water and solutions, and the ensemble average is over many initial times t_o,

$$\text{msd} = \left\langle |r(t) - r(t_0)|^2 \right\rangle_{t_0} \tag{2}$$

with $r(t)$ being the molecular position. From the msd, water oxygen diffusion coefficients, D, were calculated in the 5–20 ps interval, for which the constant slope regime has been reached, according to Einstein's relation:

$$D = \lim_{t\to\infty} \frac{1}{6t} \left\langle |r(t) - r(t_0)|^2 \right\rangle_{t_o} \tag{3}$$

We have also calculated velocity autocorrelation functions, VAF, according to equation (4):

$$C(t) = \langle v(t) \cdot v(t_0) \rangle_{t_o} \tag{4}$$

where $v(t)$ stands for the molecular velocity.

The velocity autocorrelation functions of the water solvent shown in figure 5(a) display a first minimum at ~0.1 ps, the position of the minima are unaffected by the type of the amide, only its depth is changed going from one to other amide with close values for FOR and DMF and higher value for NMF. The first maximum is also slightly different for NMF solutions being shifted to lower times. The intensity of the first peak may be assigned to the capacity of free movement of the water molecules; thus, the short time dynamics indicates that water molecules are less free to move in FOR solutions than in NMF and DMF ones. The dynamics at longer times shows the effect of the hydrophobic groups and the solvation around these moieties because the solvation shells around the hydrophobic moieties are larger than the ones around the amide oxygen [9].

The mean square displacements shown in figure 5(b) reveal that the diffusion of water in DMF solutions is slower than that in FOR and NMF. Figure 5(b) also shows that water in FOR solutions has similar mobility to pure water. The calculated diffusion coefficients of the solutions are 2.51 (FOR), 2.38 (NMF) and 2.13 (DMF) (units $10^{-9}\,m^2\,s^{-1}$), the calculated value for pure SPC-E water is 2.49 at 298 K. Thus the effect of FOR on bulk water diffusion rate is almost negligible but on the contrary NMF and especially DMF decrease the water diffusion rates as a consequence of the interaction between the water network and the hydrophobic amide groups. Hence, a remarkable effect on the dynamic properties of water is exerted by the presence of the hydrophobic *N*-substituent groups, a strong hydrogen bonding network is formed among the water molecules in the methyl group solvation shell decreasing remarkably the diffusion rate of the solvent and the freedom of movement of water molecules in the hydrophobic solvation shell. This effect is especially noteworthy for DMF because in NMF the presence of the hydrogen in the nitrogen side of the moiety gives rise to solvation structures closer to that for FOR solutions.

3.2 Acetamides

Results for the second group of molecules: ACE, NMA and DMA are analyzed in this section. The *trans* NMA isomer, is predominant both in gas phase and water solution [34,49,50], and thus is the only NMA isomer considered in our MD simulations. Another relevant feature is the existence of conformers arising from different torsional angles of the *N*-methyl group [51]; the structure reported in figure 1, in which both methyl groups are eclipsed, is the most stable in water solution. In relation to the computational models, some studies have shown that the use of fully flexible or rigid NMA has no effect on the water structure around the amide group [51].

RDFs for several atomic pairs are reported in figure 6. The acetamides–water interaction through the amide oxygen, figure 6(a), shows a pattern very similar to the one studied in the previous section for formamides. The position of the strong and sharp first peak is almost unaffected by the type of acetamide, the values of

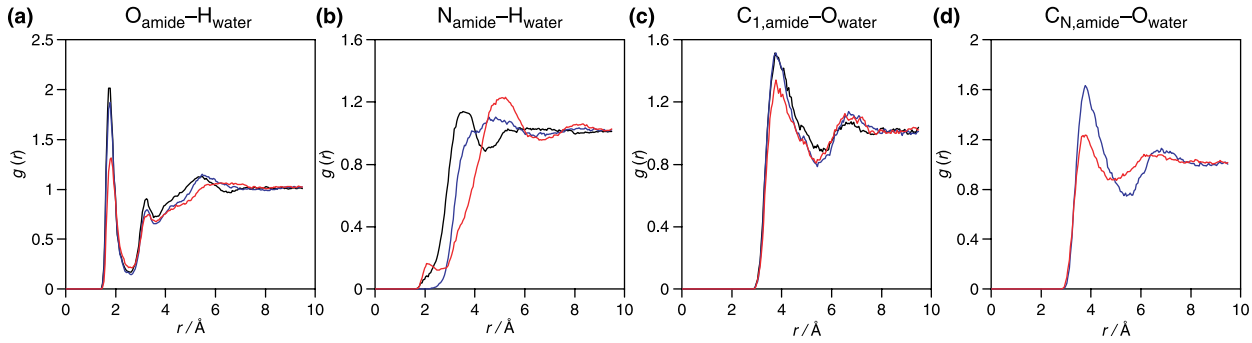

Figure 6. Calculated radial distribution functions, $g(r)$ for amide (acetamide family)—water solutions. (—) ACE, (—) NMA, (—) DMA. r = interatomic distance. $C_{1,amide}$ is the methyl carbon attached to the carbonyl carbon.

the interatomic distances at which these peaks appear reveal the existence of hydrogen bonding between amide and water molecules. The solvation numbers corresponding to these first shells, table 1 and figure 7(a), point to a 1 amide: 2 water complex through the carbonyl oxygen, as previously reported [51,52]. These solvation numbers are slightly greater for the acetamide family than for formamides (table 1); thus, the electrodonating methyl group attached to the carbonyl group reinforces the interaction with water molecules through this position. Within the acetamide family the introduction of *N*-substituents decreases the number of water molecules within the first solvation shell (table 1, $C_{1,amide}$—O_{water} and $C_{N\text{-}amide}$—O_{water}), but at the same time it reinforces the medium range solvation because of these hydrophobic moieties.

The interaction through the nitrogen side of the amide bond in acetamides is shown in figure 6(b). The RDFs reported show peaks at distances that discard hydrogen bonding directly with the nitrogen, a small feature for DMA appears at around 2 Å as for some formamides but an interaction through the nitrogen in this molecule is strongly sterically hindered and thus it should be discarded. This peak shifts to higher interatomic distances for NMA and DMA as a consequence of the hydrophobic groups. Nevertheless, the peaks are remarkably less sharp for the acetamide family than those for formamides, (figures 2(b) and 6(b)). In the case of NMA the peak is almost flat, this may be attributed to the presence of the methyl group in the carbonyl side which also reinforces the hydrophobic interactions, and to the increasing hindrance of the nitrogen atom in acetamides. The enhanced solvation numbers of the acetamide family are shown in table 1.

In the acetamide family there are two different hydrophobic moieties: the methyl group attached to the carbonyl side and the *N*-substituents. RDFs for the pairs involving the methyl group in the carbonyl side are reported in figure 6(c), which reveals strong peaks appearing at interatomic distances characteristic of hydrophobic solvation. The solvation numbers (table 1 and figure 6(c)) are very close to a complete clathrate cage (whose theoretical solvation number should be 20) which is slightly disrupted by the methyl groups in the nitrogen side as it is shown by the smaller solvation numbers of NMA and DMA, table 1 and figure 7(c).

The solvation around the methyl groups in the nitrogen side of the molecules is very similar among the formamide and acetamide families, figures 2(c) and 6(d). However the solvation numbers, table 1 and figure 7(d), are greater for acetamides and more consistent with a clathrate structure around the hydrophobic moieties. Thus, going from formamides to acetamides, the presence of the methyl group in the carbonyl side first reinforces the hydrophilic

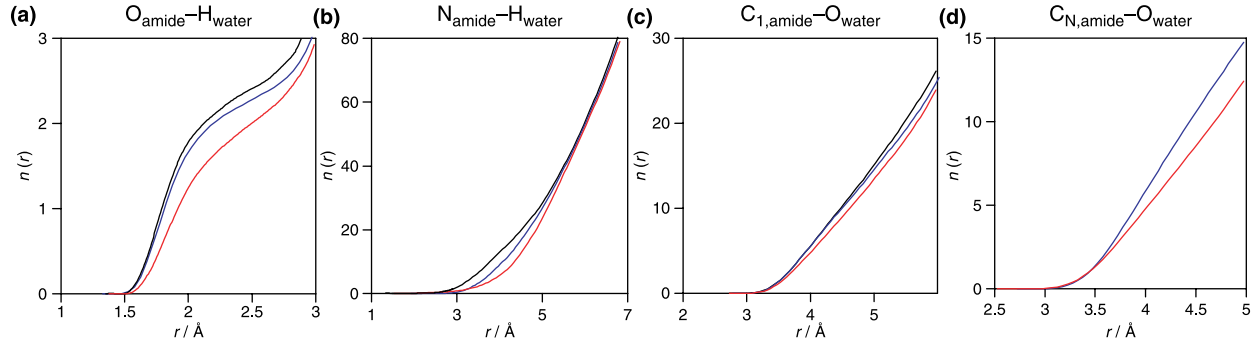

Figure 7. Number of atoms, $n(r)$, within a sphere of radius r for amide (acetamide family)—water solutions. The first atom reported in the labels for each plot is the central one. Symbols as in figure 6. r = interatomic distance.

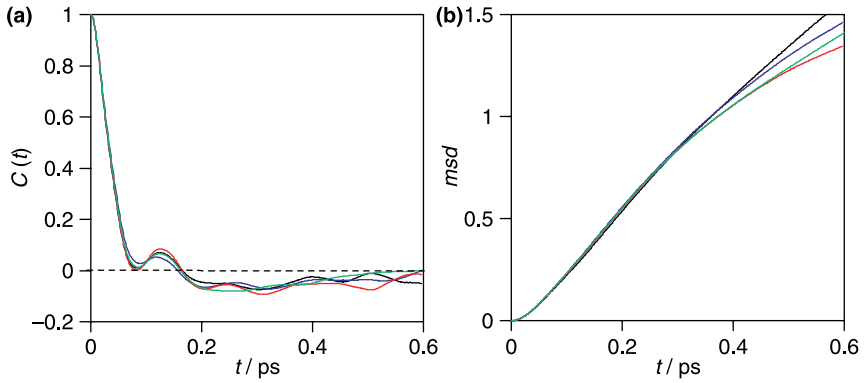

Figure 8. Velocity autocorrelation function, $C(t)$, and mean square displacement, msd/Å[2], of water oxygen atoms for amide (acetamide family)—water solutions. t = time. Symbols as in figure 6. Results for pure SPC-E water are also included, (—).

interaction through the carbonyl oxygen because of its electrodonor character, and second, gives rise to a more effective hydrophobic solvation around the different methyl groups in the molecules.

The dynamic properties of the acetamide family solutions are reported in figure 8. The velocity autocorrelation functions, figure 8(a), shows a valley and a peak at short correlation times whose main positions remain constant for all the studied acetamides changing only the corresponding intensities. The values for ACE solutions at short times are almost the same as for pure water but at longer times remarkable differences arise. DMA solution shows the deepest first valley and the higher first peak and thus this solution will show the lower diffusion rates. The msd reported in figure 8(b) shows higher diffusion rates of ACE solutions in comparison with pure water and the other acetamides, this is confirmed by the calculated diffusion constant of ACE ($2.58 \times 10^{-9}\,m^2\,s^{-1}$), slightly greater than the one for pure SPC-E water, in contrast with the lower value for DMA ($2.04 \times 10^{-9}\,m^2\,s^{-1}$). The diffusion rates and constants for DMA solutions are lower than for DMF, thus confirming the more effective hydrophobic solvation in acetamides than in formamides. Thus, *N*-substituted acetamides decrease remarkably the freedom of motion of water molecules in the solvation shells surrounding the molecule because of the strong hydrophobic solvation around all the methyl moieties.

3.3 Acrylamide

The introduction of a vinyl group into the amide moiety gives rise to several interesting features. ACA is a bifunctional molecule, the electron withdrawing capacity of the amide group gives rise to an electron-deficient vinyl double bond; these properties determine ACA's behavior in water solutions.

Some of the OPLS-AA forcefield parameters for this molecule are not available in the open literature and thus they were calculated in this work by quantum calculations at the B3LYP/6-311 + + g** level with optimized relaxed potential energy scans of the corresponding bond distances, angles or dihedrals. The calculated potential energy profiles for the different properties are then fitted to the corresponding expressions of the forcefield [23], results are reported in table 2. The forcefield reproduces properly the different contributions to the total energy, figure 9, even the torsional barrier for the transition among the *cis* and *trans* isomers is also well fitted by the model, figure 9(d).

The ACA–water interaction through the amide oxygen may be analyzed through the RDF reported in figure 10(a),

Table 2. ACA OPLS – AA parameters by fitting to calculated B3LYP/6-31 + + g** optimized relaxed potential energy scans. Units: k_r (kcal mol^{-1} Å^{-2}), r_{eq} (Å), k_θ (kcal mol^{-1} deg $^{-2}$), r_{eq} (deg), V_i (kcal mol^{-1}).

	k_r	r_{eq}	*angle*	k_θ	θ_{eq}	*Dihedral*	V_1	V_2	V_3
1–2	670.77	1.3379	1–2–5	111.61	115.05	1–2–6–7	5.048	14.650	− 5.041
1–3	402.51	1.0882	1–2–6	79.42	121.45	1–2–6–8	5.048	14.650	− 5.041
1–4	402.51	1.0882	2–1–3	55.46	121.77	2–6–8–9	− 0.885	24.247	− 0.885
2–5	393.86	1.0912	2–1–4	55.46	121.77	4–1–2–6	53.46	118.74	− 0.885
2–6	302.41	1.5031	2–6–8	112.93	123.66	5–2–1–4	0.000	4.900	0.000
6–7	817.91	1.2289	4–1–3	50.23	118.33	7–6–2–5	0.339	4.533	− 0.454
6–8	453.94	1.3729	5–2–6	62.37	118.28	7–6–8–9	0.209	3.639	1.082
8–9	523.53	1.0126	6–8–9	53.46	118.74	8–6–2–5	0.475	3.793	0.760
8–10	523.53	1.0126	6–8–10	41.68	121.70				
			7–6–8	60.44	121.03				
			9–8–10	51.77	117.73				

For atom numbering see figure 9(a). Forcefield symbols as in Ref. [23].

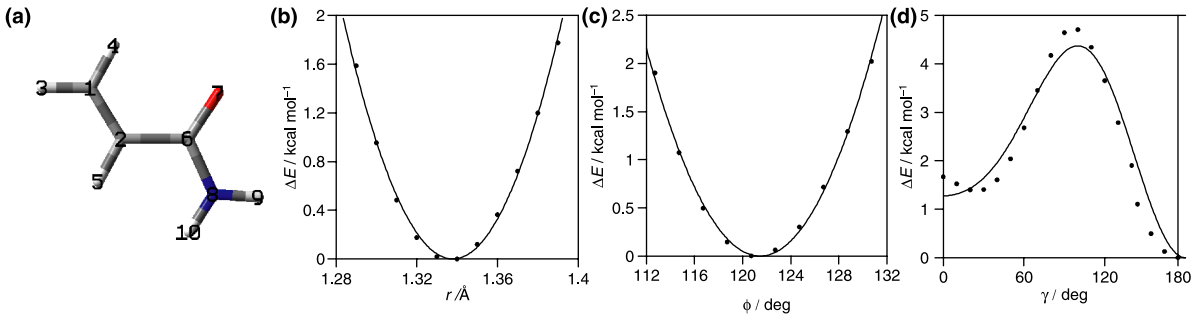

Figure 9. Potential energy scans for the bond C(═)—C(O) (1–2), angle C═C—C(O) (1–2–6) and dihedral angle C═C—C(O)—O (1–2–6–8) in ACA. r, interatomic distance, ϕ, angle, γ, dihedral angle; ΔE, energy relatives to the minimum value. (●) Calculated at B3LYP/6-311 + + g** level, (—) fitted OPLS-AA with parameters from Table 2. Color code as in figure 1.

the sharp peak, also reported previously for the other families of amides, points to strong hydrogen bonding at that amide position. The position of the first peak is close to the ones for other amides, table 1, only the peak intensity is lower but the solvation number is slightly greater for ACA because the peak is broader and therefore the first minimum of the RDF appears at slightly larger distances for ACA, figure 10(a).

The interaction through the nitrogen side of the amide group may be analyzed through figure 10(b). The RDF features (N_{amide}—H_{water}) suggest the absence of hydrogen bonding at that position. The hydrophobic solvation around the nitrogen group of ACA is more effective than in ACE as indicated by their solvation numbers, table 1 and figure 11(b).

The interaction with the carbons of the vinyl group may be analyzed through figure 10(c). The RDFs for both carbons of the vinyl group are characteristic of hydrophobic solvation; for C_1, the terminal carbon of the vinyl group, the peak appears at distances lower than for C_2, figure 10(c), showing sharper and more intense features. The solvation around this group is characteristic of a clathrate cage, table 1 and figure 11(c), and very similar to that in ACE (figures 6(c) and 10(c)), but a lower solvation number is obtained for ACA which points to a clathrate cage slightly more distorted in ACA because of the greater size of the group, but this result should be taken with care because the first minimum in RDF reported in figure 10(c) for ACA is not well defined.

Dynamic properties of ACA solutions are reported in figure 12. The behavior of the velocity autocorrelation function in ACA solutions is very similar to those previously reported for the other families of amides: a valley and a peak at very short correlation times, located at almost the same positions as in pure water, figure 12(a). The intensity of the first ACA peak is lower than that in pure SPC-E water and lower than that of ACE solutions, this first peak shows the effect of the more effective medium range solvation around the vinyl group which is confirmed by the diffusion constant in ACA solutions, $2.24 \times 10^{-9}\,m^2\,s^{-1}$, which is lower than in pure water or ACE solutions, confirming the decreasing of water freedom of motion in the ACA solvation shell. Similar features are also inferred from the msd reported in figure 12(b).

Thus, for ACA solutions, although the water–amide hydrogen bonding through the amide oxygen is less effective than in methyl substituted amides such as ACE, the hydrophobic interaction seems to be reinforced by the development of a very effective medium range solvation around the vinyl group.

3.4 Cyclic Amide

The results of MD simulations for the cyclic amides family (PYR, PIP and NMP) are reported in figures 13–15. The interaction with water through the amide oxygen may be analyzed via the RDFs reported

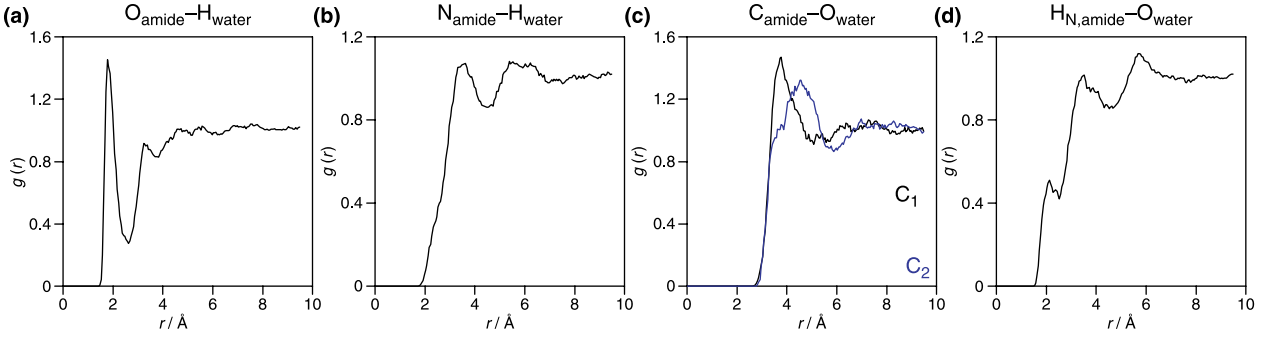

Figure 10. Calculated radial distribution functions, $g(r)$ for ACA–water solutions. r = interatomic distance. C_1 and C_2 correspond to the numbering reported in figure 9(a).

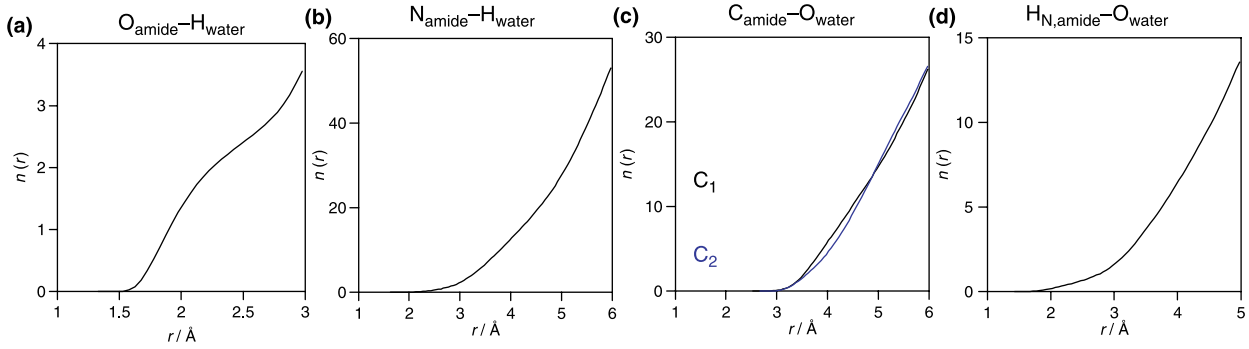

Figure 11. Number of atoms, $n(r)$, within a sphere of radius r for ACA–water solutions. The first atom reported in the labels for each plot is the central one. r = interatomic distance.

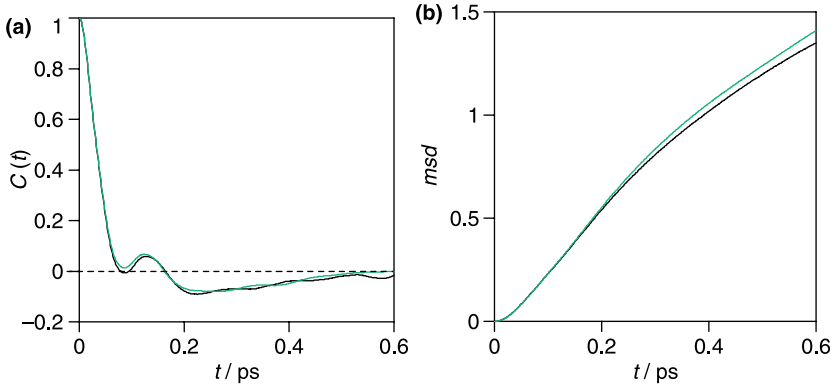

Figure 12. Velocity autocorrelation function, $C(t)$, and mean square displacement, msd/Å [2], of water oxygen atoms for ACA–water solutions. t = time. Results for pure SPC-E water are also included, (—).

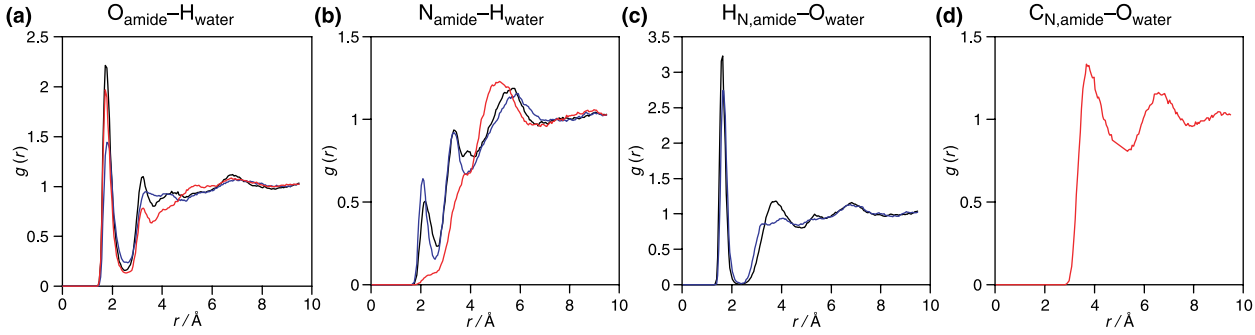

Figure 13. Calculated radial distribution functions, $g(r)$ for amide (cyclic family)—water solutions. (—) PYR, (—) PIP, (—) NMP. r = interatomic distance.

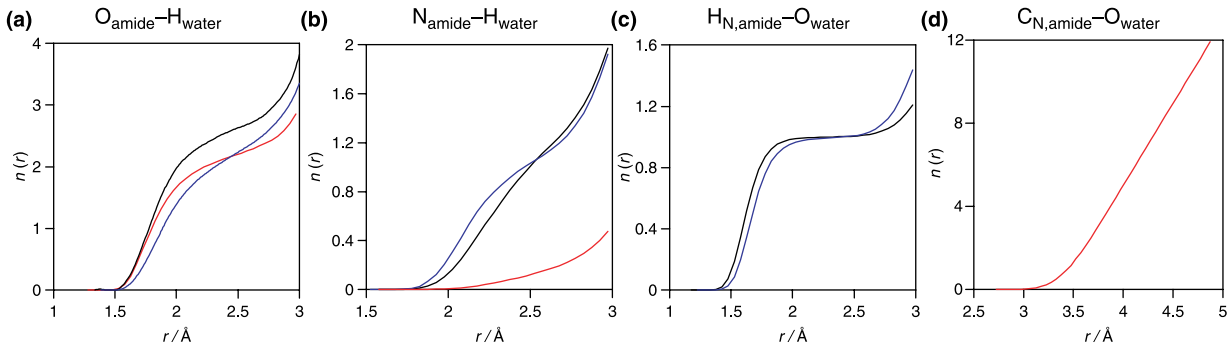

Figure 14. Number of atoms, $n(r)$, within a sphere of radius r for amide (cyclic family)—water solutions. The first atom reported in the labels for each plot is the central one. Symbols as in figure 13. r = interatomic distance.

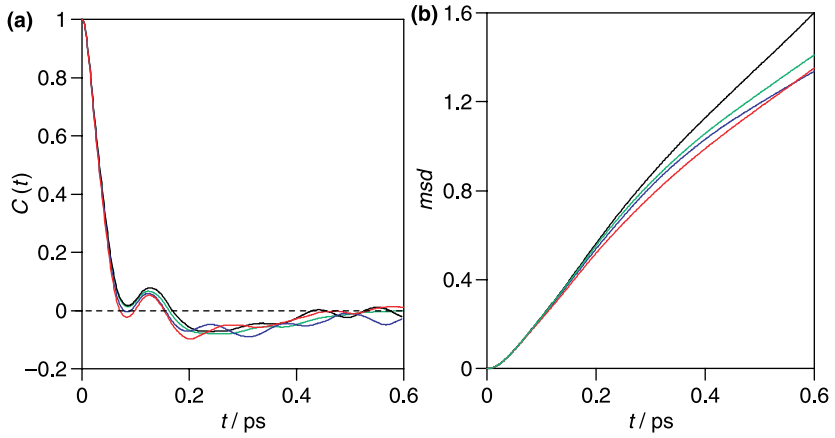

Figure 15. Velocity autocorrelation function, $C(t)$, and mean square displacement, msd/Å [2], of water oxygen atoms for amide (cyclic family)—water. t = time. Symbols as in figure 13. Results for pure SPC-E water are also included, (—).

in figure 13(a); for all the amides strong peaks at hydrogen bonding distances appear (table 1). The solvation numbers, table 1 and figure 14(a), point to 1:2 interactions with the greater number for PYR. The increase of the ring size, from PYR to PIP, decreases substantially the intensity of the first peak in RDF, and thus the solvation number, pointing to a less effective hydrogen bonding solvation for the larger ring. For NMP, the presence of methyl substituent in the amide nitrogen decreases slightly the effectiveness of the solvation in the amide oxygen compared with PYR, but this effect is less strong than that of the increase of the ring size as it is reflected by the more intense first peak in NMP compared with PIP.

The interaction through the nitrogen position is obviously very different for *N*-substituted amides than for the unsubstituted ones. A small, but well defined peak appears for PYR and PIP, figure 13(b), at distances pointing to 1:1 hydrogen bonding, table 1. A second peak is present for these molecules at longer distances pointing to a complex solvation around the amide nitrogen, but RDFs for hydrogen–water, figure 13(c) and table 1, confirm clearly the hydrogen bonding of the amide bond. For NMP, the solvation around the nitrogen position indicates clearly a hydrophobic solvation, figure13(b), (d), the solvation number is characteristic of clathrate cages, table 1 and figure 14(d), slightly disrupted by the cyclic shape of the molecule.

The dynamic properties of these solutions are reported in figure 15. The velocity autocorrelation functions, figure 15(a), show the first valley and peak at very short times as for the previously reported amides, but the behaviour of PYR solutions is slightly different to the other ones. The trend obtained in velocity autocorrelations functions for PYR solutions is very similar to pure SPC/E water, only the first peak is slightly greater than in pure water. This behavior is confirmed by the msd (figure 15(b)), yielding a diffusion constant of $2.54 \times 10^{-9}\,m^2\,s^{-1}$ for water in PYR solutions. Thus, in spite of the strong interaction between water and PYR through the oxygen and nitrogen position of the amide ring, the medium range hydrophobic solvation is less efficient than for the other cyclic amides considered. The calculated PIP and NMP diffusion constants are 2.40×10^{-9} and $2.06 \times 10^{-9}\,m^2\,s^{-1}$ respectively, showing that the introduction of hydrophobic substituents in the amide molecules is more effective for reducing the water mobility in the first solvation sphere than increasing the ring size is. Thus, both effects reinforce the solvation through the development of hydrophobic solvation cages.

3.5 *Visualization of water clustering around amides*

Finally, a visual inspection of the clustering structure around the hydrophobic and hydrophilic regions of amides was done from representative MD snapshots. From the results reported in the previous sections it is clear that the water hydrogen bonding network suffers a rearrangement around the hydrophobic and hydrophilic parts of amide molecules giving rise to effective solvation around these amide moieties. In order to visualize the water structure around amide molecules spherical cutoffs with different radius centered in the amide carbon (C═O) were analyzed. Figure 16 shows results of this analysis for NMA, showing strong water ordering not only around the hydrophilic moiety but also an important structuring effect around the hydrophobic groups. Visual inspection of the water organization in figure 16(c) reveals a rich hydrogen-bond network creating a cagelike structure around the amide molecule, similar results are obtained for the remaining linear amides and we may conclude that amides act as structuring molecule in the surrounding water structure. For cyclic amides of larger size a similar effect is obtained. Figure 17 illustrates that the water in the solvation shell is also structured around the hydrophobic groups attached to the rings and an effective cagelike structure around the cycle is formed.

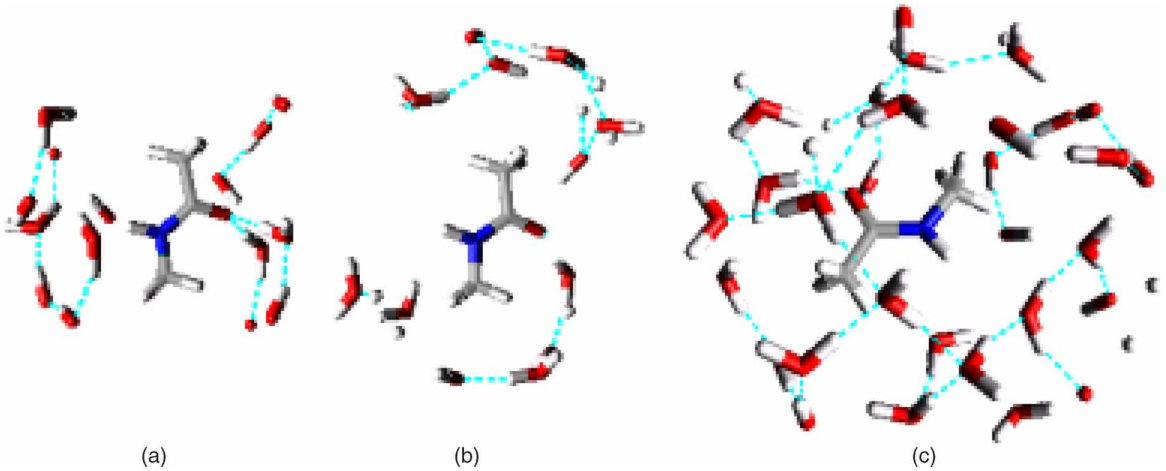

Figure 16. Representative snapshots of water clustering in NMA/water mixtures around (a) hydrophilic, (b) hydrophobic NMA molecular parts and (c) whole NMA molecule. Color code as in figure 1.

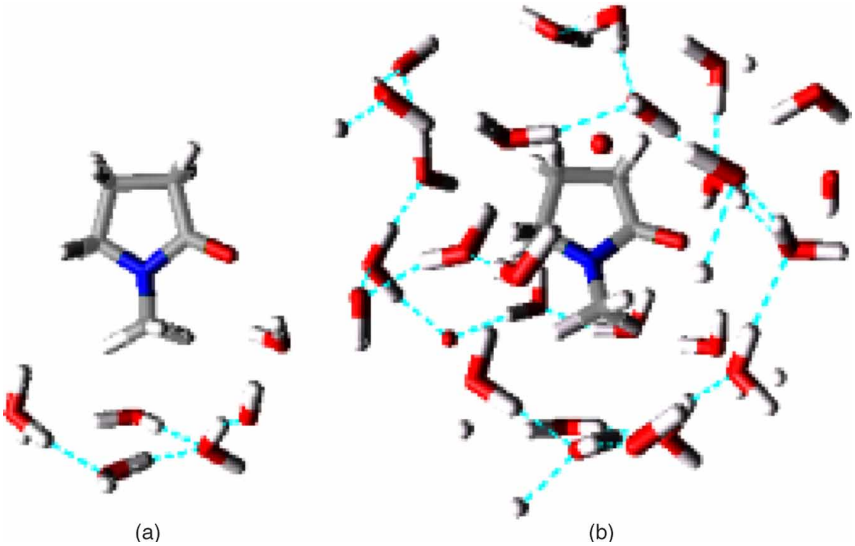

Figure 17. Representative snapshots of water clustering in NMP/water mixtures around (a) hydrophobic NMP molecular parts and (c) whole NMP molecule. Color code as in figure 1.

4. Conclusions

The structure of infinitely diluted amide–water solutions is studied for different families of compounds using MD simulations. The results obtained point to strong solvation structures around the amide molecules, with hydrogen bonding interactions mainly through the amide oxygen, and with hydrophobic solvation around the nitrogen groups, alkyl radicals and cyclic groups. The analysis of the solvation numbers suggests the formation of clathrate type structures disrupted by the different sizes and shapes of the involved molecules. The structural and dynamical properties of water surrounding the studied amides suggest that these molecules cause a very remarkable effect on the adjacent water structure acting as structure-creating molecules. Short-range effects are dominating for this kind of systems, therefore, this structure-creating ability is mainly of local nature in spite of the fact than more than one solvation shells are formed around the studied amides. The ability of amide molecules to reinforce the water liquid structure, evidenced by the behavior of their dynamic properties, may compete with the process in which clathrate cages around small gas molecules are growing and thus contributing to delay the clathrate formation. Further studies are being carried out in which the simultaneous interaction of the inhibitor monomers with solid clathrates and liquid water is analyzed.

Acknowledgements

We gratefully acknowledge financial support from: Texas A&M University, the USA—Spain Fulbright Commission and Ministerio de Educación y Ciencia (Spain) (SAM), and the Gas Processors Suppliers Association (GPSA).

References

[1] E.D. Sloan. *Clathrate Hydrates of Natural Gases*, 2nd ed., Marcel Dekker, New York (1998).

[2] E.G. Hammerschmidt. *Ind. Eng. Chem. Res.*, **26**, 851 (1934).

[3] J. Carroll. *Natural Gas Hydrates*, Elsevier, Amsterdam (2003).

[4] F.E. Anderson, J.M. Prausnitz. Inhibition of gas hydrates by methanol. *AIChE J.*, **32**, 1321 (1986).

[5] Y.F. Makogon, T.Y. Makogon, S.A. Holditch. Kinetics and mechanisms of gas hydrate formation and dissociation with inhibitors. *Ann. NY Acad. Sci.*, **912**, 777 (2000).

[6] C.A. Koh, R.E. Westacott, W. Zhang, K. Hirachand, J.L. Creek, A.K. Soper. Mechanisms of gas hydrate formation and inhibition. *Fluid Phase Equilib.*, **194**, 143 (2002).

[7] E.D. Sloan, S. Subramanian, P.N. Metthews, J.P. Lederhos, A.A. Khokar. Quantifying hydrate formation and kinetic inhibition. *Ind. Eng. Chem. Res.*, **37**, 3124 (1998).

[8] C.A. Koh. Towards a fundamental understanding of natural gas hydrates. *Chem. Soc. Rev.*, **31**, 157 (2002).

[9] T.J. Carver, M.G.B. Drew, P.M. Rodger. Molecular dynamics calculations of N-methylpyrrolidone in liquid water. *Phys. Chem. Chem. Phys.*, **1**, 1807 (1999).

[10] M.T. Storr, P.C. Taylor, J.P. Monfort, P.M. Rodger. Kinetic inhibitor of hydrate crystallization. *J. Am. Chem. Soc.*, **126**, 1569 (2004).

[11] M.T. Storr, P.M. Rodger, J.P. Montfort, L. Jussaume. A mechanistic study of low dosage inhibitors of clathrate hydrate formation. *Foundations of Molecular Modeling and Simulation*, AIChE Symposium Series No 325 (2001).

[12] B.J. Anderson, J.W. Tester, G.P. Borghi, B.L. Trout, B.L. Am. Properties of inhibitors of methane hydrate formation via molecular dynamics simulations. *J. Chem. Soc.*, **127**, 17852 (2005).

[13] M.A. Kelland, T.M. Svartaas, J. Ousthus, T. Namba. A new class of kinetic hydrate inhibitor. *Ann. NY Acad. Sci.*, **912**, 281 (2000).

[14] B. Kvamme, T. Kuznetsova, K. Aaasoldsen. Molecular dynamics simulations for selection of kinetic hydrate inhibitors. *J. Mol. Graph. Modell.*, **23**, 524 (2005).

[15] W. Smith, T.R. Forester. DL_POLY_2.0: A general-purpose parallel molecular dynamics simulation package. *J. Mol. Graph.*, **14**, 136 (1996).

[16] W.G. Hoover. Canonical dynamics: equilibrium phase-space distributions. *Phys. Rev.*, **A31**, 1695 (1985).

[17] M.P. Allen, D.J. Tildesley. *Computer Simulation of Liquids*, Clarendon Press, Oxford, UK (1989).

[18] J.P. Rickaert, G. Ciccotti, H.J. Berendsen. Numerical-integration of cartesian equations of motion of a system with constraints - molecular-dynamics of N-alkanes. *J. Comput. Phys.*, **23**, 327 (1977).

[19] U.L. Essmann, M.L. Perera, T. Berkowitz, H. Darden, H. Lee, L.G. Pedersen. A smooth particle mesh Ewald method. *J. Chem. Phys.*, **103**, 8577 (1995).

[20] H.J. Berendsen, J.R. Grigera, T.P. Straatsma. The missing term in effective pair potentials. *J. Phys. Chem.*, **91**, 6269 (1987).

[21] Y. Guissani, B. Guillot. A computer-simulation study of the liquid-vapor coexistence curve of water. *J. Chem. Phys.*, **98**, 8221 (1993).

[22] M.C. Bellisent-Funel, T. Tassaing, H. Zhao, D. Beysens. The structure of supercritical heavy water as studied by neutron diffraction. *J. Chem. Phys.*, **107**, 2942 (1997).

[23] W.L. Jorgensen, D.S. Maxwell, J. Tirado-Rives. Development and testing of the OPLS all-atom force field on conformational energetics and properties of organic liquids. *J. Am. Chem. Soc.*, **118**, 11225 (1996).

[24] R.C. Rizzo, W.L. Jorgensen. OPLS all-atom model for amines: Resolution of the amine hydration problem. *J. Am. Chem. Soc.*, **121**, 4827 (1999).

[25] N.A. McDonald, W.L. Jorgensen. Development of an all-atom force field for heterocycles. Properties of liquid pyrrole, furan, diazoles, and oxazoles. *J. Phys. Chem. B*, **102**, 8049 (1998).

[26] G. Kaminski, E.M. Duffy, T. Matsui, W.L. Jorgensen. Free-Energies of hydration and pure liquid properties of hydrocarbons from the Opls all-atom model. *J. Phys. Chem.*, **98**, 13077 (1994).

[27] J.L. McCallum, D.P. Tieleman. Calculation of the water-cyclohexane transfer free energies of neutral amino acid side-chain analogs using the OPLS all-atom force field. *J. Comput. Chem.*, **24**, 1930 (2003).

[28] R. Zhang, H. Li, Y. Lei, S. Han. Different weak C-H center dot center dot O contacts in N-methylacetamide-water system: Molecular dynamics simulations and NMR experimental study. *J. Phys. Chem. B*, **108**, 12596 (2004).

[29] M.J. Frisch, G.W. Trucks, H.B. Schlegel, G.E. Scuseria, M.A. Robb, J.R. Cheeseman, V.G. Zakrzewski, J.A. Montgomery, R.E. Stratmann, J.C. Burant, S. Dapprich, J.M. Millam, A.D. Daniels, K.N. Kudin, M.C. Strain, O. Farkas, J. Tomasi, V. Barone, M. Cossi, R. Cammi, B. Mennucci, C. Pomelli, C. Adamo, S. Clifford, S. Ochterski, G.A. Petersson, P.I. Ayala, Q. Cui, K. Morokuma, P. Salvador, J.J. Dannenberg, D.K. Malick, A.D. Rabuck, K. Raghavachari, J.B. Foresman, J. Cioslowski, J.V. Ortiz, A.G. Baboul, B.B. Stefanov, G. Liu, A. Liashenko, P. Piskorz, I. Komaromi, R. Gomperts, R.L. Martin, D.J. Fox, T. Keith, M.A. Al-Laham, C.Y. Peng, A. Nanayakkara, M. Challacombe, P.M.W. Gill, B. Johnson, W. Chen, M.W. Wong, J.L. Andres, C. Gonzalez, M. Head-Gordon, E.S. Replogle, J.A. 20019 Pople. *Gaussian 98 (Revision A.11.3)*, Gaussian, Inc., Pittsburgh PA (2001).

[30] A.D. Becke. Density-functional exchange-energy approximation with correct asymptotic-behavior. *Phys. Rev. A*, **38**, 3098 (1988).

[31] C. Lee, W. Yang, R.G. Parr. Development of the Colle-Salvetti correlationenergy formula into a functional of the electron density. *Phys. Rev. B*, **37**, 785 (1988).

[32] A.D. Becke. Density-functional thermochemistry .3. The role of exact exchange. *J. Chem. Phys.*, **98**, 5648 (1993).

[33] B.H. Besler, K.M. Merz, P.A. Kollman. Atomic charges derived from semiempirical methods. *J. Comput. Chem.*, **11**, 431 (1990).

[34] S. Aparicio-Martínez, K.R. Hall, P.B. Balbuena. Theoretical study on the properties of linear and cyclic amides in gas phase and water solution. *J. Phys. Chem. A*, **110**, 9183 (2006).

[35] H. Yeleker, A. Guven, R. Ozkan. Hydrogen bonding and dimeric selfassociation of 2-pyrrolidinone: An *ab initio* study. *J. Comp. Aided. Mol. Des.*, **13**, 589 (1999).

[36] X. Huang, C.J. Margulis, B.J. Berne. Do molecules as small as neopentane induce a hydrophobic response similar to that of large hydrophobic surfaces?. *J. Phys. Chem. B*, **107**, 11742 (2003).

[37] A. Vishnyakov, A.P. Lyubartsev, A. Laaksonen. Molecular dynamics simulations of dimethyl sulfoxide and dimethyl sulfoxide-water mixture. *J. Phys. Chem. A*, **105**, 1702 (2001).

[38] A. García-Martínez, E. Teso-Villar, A. García-Fraile, P. Martínez-Ruiz. A computational and experimental study on the relative stabilities of cis and trans isomers of N-alkylamides in gas phase and in solution. *J. Phys. Chem. A*, **106**, 4942 (2002).

[39] A. Radzicka, L. Pedersen, R. Wolfenden. Influences of solvent water on protein folding - free-energies of solvation of cis and trans peptides are nearly identical. *Biochemistry*, **27**, 4538 (1988).

[40] G. Nandini, D.N. Sathyamarayana. *Ab initio* studies on geometry and vibrational spectra of N-methyl formamide and N-methylacetamide. *J. Mol. Stru. Theochem*, **579**, 1 (2002).

[41] K.B. Wiberg, D.J. Rush. Methyl rotational barriers in amides and thioamides. *J. Org. Chem.*, **67**, 826 (2002).

[42] A.C. Fantoni, W. Caminati. Rotational spectrum and *ab initio* calculations of N-methylformamide. *J. Chem. Soc. Faraday Trans.*, **92**, 343 (1996).

[43] S. Chalmet, M.F. Ruiz-Lopez. Molecular dynamics simulation of formamide in water using density functional theory and classical potentials. *J. Chem. Phys.*, **111**, 1117 (1999).

[44] J.S. Craw, J.M. Guest, M.D. Cooper, N.A. Burton, I.H. Hillier. Effect of hydration on the barrier to internal rotation in formamide. Quantum mechanical calculations including explicit solvent and continuum models. *J. Phys. Chem.*, **100**, 6304 (1996).

[45] J. Gao. Potential of mean force for the isomerization of Dmf in aqueous-solution - a Monte-Carlo Qm/Mm simulation study. *J. Am. Chem. Soc.*, **115**, 2930 (1993).

[46] W.L. Jorgensen, C.J. Swenson. Optimized intermolecular potential functions for amides and peptides - hydration of amides. *J. Am. Chem. Soc.*, **107**, 1489 (1985).

[47] A.K. Soper. The radial distribution functions of water and ice from 220 to 673 K and at pressures up to 400 MPa. *Chem. Phys.*, **258**, 121 (2000).

[48] C. Vega, C. McBride, E. Sanz, J.L.F. Abascal. Radial distribution functions and densities for the SPC/E, TIP4P and TIP5P models for liquid water and ices I-h, I-c, II, III, IV, V, VI, VII, VIII, IX, XI and XII. *Phys. Chem. Chem. Phys.*, **7**, 1450 (2005).

[49] S. Ataka, H. Takeuchi, M. Tasumi. Infrared studies of the less stable Cis form of N-methylformamide and N-methylacetamide in low-temperature nitrogen matrices and vibrational analyses of the trans and Cis forms of these molecules. *J. Mol. Struct.*, **113**, 147 (1984).

[50] Y.A. Mantz, H. Gerard, R. Iftimie, G.Y. Martyna. Lsomerization of a peptidic fragment studied theoretically in vacuum and in explicit water solvent at finite temperature. *J. Am. Chem. Soc.*, **126**, 4080 (2004).
[51] B. Mennucci, J.M. Martínez. How to model solvation of peptides?Insights from a quantum-mechanical and molecular dynamics study of N-methylacetamide. 1. Geometries, infrared, and ultraviolet spectra in water. *J. Phys. Chem. B*, **109**, 9818 (2005).
[52] E.M. Duffy, D.L. Severance, W.L. Jorgensen. Solvent effects on the barrier to isomerization for a tertiary amide from *ab initio* and Monte-Carlo calculations. *J. Am. Chem. Soc.*, **114**, 7535 (1992).